



OPEN

SUBJECT AREAS:
NEUROSCIENCE
MECHANISMS OF DISEASEReceived
29 September 2014Accepted
16 December 2014Published
20 January 2015Correspondence and
requests for materials
should be addressed to
S.T.H. (hou.st@sustc.
edu.cn)

Semaphorin3A elevates vascular permeability and contributes to cerebral ischemia-induced brain damage

Sheng Tao Hou^{1,2,3}, Ladan Nilchi^{2,3}, Xuesheng Li^{2,3}, Sandhya Gangaraju³, Susan X. Jiang³, Amy Aylsworth³, Robert Monette³ & Jacqueline Slinn³¹Department of Biology, South University of Science and Technology of China, 1088 Xueyuan Blvd, Nanshan District, Shenzhen, P.R. China, 518055, ²Department of Biochemistry, Microbiology and Immunology, University of Ottawa, Ottawa, Ontario, Canada, ³Human Health Therapeutics Portfolio, National Research Council Canada, 1200 Montreal Road, Bldg M54, Ottawa, Ontario, K1A 0R6, Canada.

Semaphorin 3A (Sema3A) increased significantly in mouse brain following cerebral ischemia. However, the role of Sema3A in stroke brain remains unknown. Our aim was to determine whether Sema3A functions as a vascular permeability factor and contributes to ischemic brain damage. Recombinant Sema3A injected intradermally to mouse skin, or stereotactically into the cerebral cortex, caused dose- and time-dependent increases in vascular permeability, with a degree comparable to that caused by injection of a known vascular permeability factor vascular endothelial growth factor receptors (VEGF). Application of Sema3A to cultured endothelial cells caused disorganization of F-actin stress fibre bundles and increased endothelial monolayer permeability, confirming Sema3A as a permeability factor. Sema3A-mediated F-actin changes in endothelial cells were through binding to the neuropilin2/VEGFR1 receptor complex, which in turn directly activates Mical2, a F-actin modulator. Down-regulation of Mical2, using specific siRNA, alleviated Sema3A-induced F-actin disorganization, cellular morphology changes and endothelial permeability. Importantly, ablation of Sema3A expression, cerebrovascular permeability and brain damage were significantly reduced in response to transient middle cerebral artery occlusion (tMCAO) and in a mouse model of cerebral ischemia/haemorrhagic transformation. Together, these studies demonstrated that Sema3A is a key mediator of cerebrovascular permeability and contributes to brain damage caused by cerebral ischemia.

Increased vascular permeability occurs during cerebral ischemia/reperfusion injury resulting in neuronal damage and prolonged loss of brain functions^{1–4}. Therefore, identification of factors regulating vascular permeability in stroke brain is of clinical importance in developing therapeutics to stroke.

Our previous studies demonstrated elevated brain expression of Semaphorin 3A (Sema3A) and its receptor neuropilin 1 (NRP1) during cerebral ischemia and reperfusion^{5–9}. Other studies also demonstrated elevated expression of Sema3A and NRP1 in the component of the scar tissue in stroke brain^{10–14}. Sema3A induces VE-cadherin serine phosphorylation and internalisation, cell-cell junction destabilisation, and loss of barrier integrity in brain endothelial cells¹⁵. However, whether and how Sema3A participates in cerebral ischemia-induced brain damage remains unclear.

Produced by both neurons and glial cells of the scar tissue^{5,16,17}, elevated Sema3A causes neuronal death through NRP1 receptors^{7,8,14}. Hypoxic neurons in ischemic retina also secrete Sema3A to inhibit retina vascular regeneration^{18,19}. Indeed, during development, Sema3A not only inhibits axonal outgrowth^{20–22}, but also blood vessel patterning^{23,24}. It is therefore not surprising that Sema3A participates in tumor development through inhibiting endogenous angiogenesis^{15,25–27}.

Cellular receptors for Sema3A are NRPs^{28,29}, which contains NRP1 and NRP2. NRPs are non-tyrosine kinase trans-membrane receptors with a short intracellular domain lacking of any signalling motifs. Therefore, NRPs participate in signal transduction as co-receptors with plexins or vascular endothelial growth factor receptors (VEGFR) to inhibit axonal outgrowth and to guide the development of blood vessels, respectively^{24,30,31}. Vascular endothelial cells express NRPs. Together with specific isoforms of VEGFRs, NRPs mediate vascular response to Sema3A during vasculogenesis, angiogenesis, and vascular remodeling^{30,32,33}.



Mical proteins are molecular conduit through which *Sema3A* affects actin reorganization in *Drosophila*^{34,35}. Alteration of the actin cytoskeleton produces hallmarks of cell morphological changes, such as loss of polarity and the appearance of rounded shapes^{34,36,37}. Micals are an evolutionary conserved family of multidomain signal transduction proteins³⁷, and which can directly modify actin cytoskeleton depending on their monooxygenase enzyme activity and/or redox signaling^{34,35,37}.

In the present study, we show *Sema3A* increases vascular permeability mediated through NRP2/VEGFR1 receptors. In response to *Sema3A*, VEGFR1 directly interacts with Mical2 to cause F-actin disorganization, thereby changing cerebroendothelial cell morphology and permeability. Deletion of *Sema3A* expression (*Sema3A*^{-/-} mice) reduced cerebrovascular permeability and protected mouse brain against two types of cerebral ischemia.

Methods

Materials. All chemicals and reagents, unless stated otherwise, were purchased from Sigma Chemical Co. (Burlington, ON, Canada) and were of analytical grade or higher. Recombinant *Sema3A* was purchased from R&D Systems (Minneapolis, MN). A battery of primary antibodies were purchased from commercial sources and used for blocking experiments and Western blots (WB) as shown in the Table 1. Chemical inhibitors Zm 306416 (Catalog No. S2897, specific for VEGFR1) and Ki8751 (specific for VEGFR2) were purchased from Selleckchem.com.

Animals. All procedures using animals were approved by the Institute for Biological Sciences Animal Care Committee (protocol 2007.13) following the guidelines established by the Canadian Council on Animal Care. Sprague Dawley male rats (200–250 g) were obtained from Charles River (St Foie, PQ, Canada). *Sema3A* knockout (*Sema3A*^{-/-}; backcrossed with C57BL/6) mice were kind gifts from Dr Masahiko Taniguchi (Sapporo Medical University, Japan) as described previously³⁸. *Sema3A*^{-/-} mice were bred by mating between heterozygote littermates and genotyped using PCR exactly as previously described³⁸. Only male *Sema3A*^{+/+}, *+/+* and *-/-* littermate mice were used for the study.

Miles assay and measurement of Evans blue in tissue. *Sema3A*^{+/+} mice weighing 30 g were used in this experiment. First, Evans blue dye (100 µl, 1.5%) was injected through the lateral tail vein. After 10 min of circulation, 10 µl of PBS, VEGF (diluted in PBS), or *Sema3A* (diluted in PBS) were injected intradermally into the middle dorsal part of ears, or into the shaved abdominal skin. After different time periods, image analysis was performed and the tissue was collected under anaesthesia for Evans blue extraction analysis. To do this, tissues were removed, weighted and fixed for 48 h in 1 ml of 4% formaldehyde at 60°C to extract Evans blue from the tissue. Evans blue dye concentration was measured using a spectrophotometer at 600 nm and the value obtained was reported as OD₆₀₀/mg of tissue. For the Miles assay, after Evans blue dye injection, 100 µl of PBS, human recombinant VEGF, or *Sema3A* was injected intradermally in mice or rats. The appearance of blue spots was monitored, photographed and quantified as described above.

Brain injury using needle puncture. *Sema3A*^{-/-}, *Sema3A*^{+/+}, and *Sema3A*^{+/+} male littermate mice (25 g in body weight) were injected with 100 µl of 1.5% Evans Blue dye through the lateral tail vein. After 10 min of circulation, a puncture was made to the left hemisphere of each brain with a 26 gauge needle using a stereotactic injection device. Two hours later, mice were anesthetized and perfused through the left heart ventricle with 30 ml ice cold 1 X PBS, followed by 10 ml of 4% paraformaldehyde. Mouse brain was removed and put into 4% formaldehyde overnight. The amount of Evans blue dye in the brain was extracted and quantified as described above.

Unilateral transient middle cerebral artery occlusion (tMCAO) and reperfusion in mouse. Under temporary isoflurane anaesthesia, mice were subjected to a 60 min tMCAO using an intraluminal filament as previously described^{6,7,39,40}. After 30 min of

tMCAO, the filament was withdrawn and blood flow was restored to basal levels, as assessed by laser Doppler flowmetry. Wounds were sutured following surgery. The body temperature of experimental mice was monitored before and after the tMCAO surgery using a rectal probe and was maintained at 37°C using a heating pad and lamp. In preliminary, experiments to verify a consistent stroke procedure, measurements of blood pressure, blood gases, and pH were also performed. Sham-operated mice were subjected to the same surgery without tMCAO and used as controls. Mice were allowed to recover for 24 h following tMCAO and during this period, body weight and neurological functions were measured.

Photothrombotic occlusion/hemorrhagic transformation model. Endothelial injury in cerebral blood vessels was induced using a photochemical method with some modifications^{41,42}. Mice were anesthetized and a small cut (10 mm) was made on the left side of the head to expose the skull. Mice were injected through the tail vein with a rose bengal solution, followed by photo-irradiation through the skull with a xenon lamp equipped with a heat-absorbing filter (excitation wavelength at 530–550 nm of 30 mW) for 20–30 min through a 10 X microscope objective. After the surgery, wound was surgical dressed. Mouse was allowed to go back to the cage and fed with water and food *ad libitum*. Mice were sacrificed 24 h–7 d after the surgery. Brains were removed, sliced and stained with TTC. The total haemorrhagic areas from all brain sections were calculated by computer analysis. Another set of fresh brain tissue was also collected for biochemical analysis.

Brain tissue processing and sectioning. Brain tissue was processed as previously described⁴³. Briefly, at various reperfusion time points, mice were anesthetized with isoflurane and perfused transcardially first with saline followed by 4% formaldehyde in PBS. Brains were removed, post fixed in 4% formaldehyde (pH 7.4) for 18 h and cryoprotected in 30% sucrose for 36 h at 4°C. Coronal sections (10 µm thickness) were cut using a cryostat (Leica Microsystems, Wetzlar, Germany) and mounted on superfrost slides (Fisher Scientific, Toronto, ON, Canada), stored at –80°C.

Immunohistochemistry and image quantification. Immunohistochemistry was performed exactly as we previously described⁴⁰. Immunostained sections were visualized on a Zeiss inverted microscope and digital images were obtained using the Axiovision v.4.7.2.0 software as we previously described^{6,39,44}. High resolution (1300 × 1300 d.p.i.) individual color layers were imported into NIH Image J software (<http://rsb.info.nih.gov/ij/>) and converted into grey scale mode. A common threshold was established for all images for image intensity analysis. At least five randomly selected areas were measured and averaged. All experiments were repeated at least three times.

Generation and purification of replication defective adenovirus for injection. The methods used to generate replication defective adenovirus were exactly as previously described^{45,46}. Replication defectiverecombinant adenoviruses were generated from the constructed pShuttle transfer vectors using the AdEasy vector system (QBiogene) according to the manufacturer's instructions. Human embryonic kidney 293A cells (HEK-293A) (Q Biogene, Carlsbad, CA) were cultured in Dulbecco's modified Eagle medium (DMEM) supplemented with 10% fetal calf serum and 40 µg/ml gentamycin sulfate. The identity of all recombinant adenoviruses was confirmed by PCR amplification and EGFP fluorescence. Recombinant constructs were verified by sequencing and recombinant adenoviral particles were CsCl purified and titrated as described previously^{45,46}. To prepare for injection of the viral particles, Ad viruses were subjected to two rounds of CsCl₂ ultracentrifugation purification and extensive dialysis to remove the CsCl₂.

In vitro culture of rat brain capillary endothelial cells (RBEC). Primary cultures of RBEC were prepared from 3-week-old rats, as previously described⁴⁷. Meninges were carefully removed from forebrains and gray matter was minced into small pieces of approximately 1 mm³ in ice-cold Dulbecco's modified Eagle's medium (DMEM), then dissociated by 25-times of up- and down-strokes with a 5-ml pipette in DMEM containing collagenase type 2 (1 mg/ml, Worthington Biochemical Corp., NJ, USA), 300 µl DNase (15 µg/ml), gentamycin (50 µg/ml) and then digested in a shaker for 1.5 h at 37°C. The cell pellet was separated by centrifugation in 20% bovine serum albumin (BSA)-DMEM (1000 × g, 20 min). The microvessels obtained in the pellet were further digested with collagenase-dispase (1 mg/ml, Roche Applied Sciences, Basel, Switzerland) and DNase (6.7 µg/ml) in DMEM for 1 h at 37°C. Microvessel

Table 1 | Source of primary antibodies and the amount used

Antibody	Source	Catalogue Number	Amount Used
Anti-Sema3A	Santa Cruz	sc-1148	2 µg (blocking)
Anti-Neuropilin 1	Calbiochem	PC343	2 µg (blocking)
Anti-Neuropilin 2	Zymed	361500	2 µg (blocking)
Anti-Plexin A1	Santa Cruz	sc-25639	2 µg (blocking)
Anti-VEGFR1	R&D Systems	AF471	2 µg (blocking)
Anti-VEGFR2	R&D Systems	AF644	2 µg (blocking)
Anti-hemoglobin subunit alpha	abcam	Ab92492	2 µg (WB)
Anti-CRMP3	gift		J Kappler (Germany)



endothelial cell clusters were separated on a 33% continuous Percoll (Pharmacia, Uppsala, Sweden) gradient, collected and washed twice in DMEM before plating on 35 mm plastic dishes coated with collagen type IV and fibronectin (both 0.1 mg/ml). RBEC cultures were maintained in DMEM/F12 supplemented with 10% plasma derived serum (PDS, Animal Technologies Inc., MD, USA), basic fibroblast growth factor (bFGF, Roche, Applied Sciences, Basel, Switzerland, 1.5 ng/mL), heparin (100 µg/ml), insulin (5 µg/ml), transferrin (5 µg/ml), sodium selenite (5 ng/ml) (insulin-transferrin-sodium selenite media supplement), gentamycin (50 µg/ml) and puromycin (4 µg/ml) (RBEC medium I) at 37°C with a humidified atmosphere of 5% CO₂/95% air, for 2 days. On the third day, the cells received a new medium which contained all the components of RBEC medium I except puromycin (RBEC medium II). When the cultures reached 80% confluency (4th day in vitro), the purified endothelial cells were passaged by a brief treatment with trypsin (0.05%, w/v)-EDTA (0.02%, w/v) solution, and used in vitro BBB models.

Phalloidin staining. RBEC were cultured in a 24 well plate on glass coverslips. Cells grew vigorously and did not appear to enter quiescence and de-activation even at relatively low density. Cells were subjected to the following treatment: 1) Sema3A treatment: 0.2, 1, 2, 5 or 10 µg recombinant Sema3A was added into 200 µl medium. Cells were treated for 1 h; 2) Denatured Sema3A treatment: Sema3A (2 µg) was denatured in the boiling water for 10 min. After it was cooled to room temperature, denatured Sema3A was added into cells for 1 h; 3) Antibody pre-treatment: specific antibodies to Neuropilin 1, Neuropilin 2, PlexinA1, VEGFR1 or VEGFR2 (2 µg) were added to 200 µl cell culture medium to treat cells for 1 h, followed by Sema3A (2 µg) treatment for another 1 h.

After these treatments, the culture medium was removed and the cells were fixed in freshly prepared 4% formaldehyde (in 1 X PBS) for 20 min. Cells were washed in PBS twice, 5 min each, incubated with blocking solution (1.5% BSA in PBS, containing 0.2% Triton X-100 and 0.02% Na₂S₂O₈) for 30 min, and stained with rhodamine labelled phalloidin (1:100, in blocking solution) for 1 h. After washing with PBS (3 min each for 3 times), deionized water (once), cells were mounted in Dako mounting medium (spiked with Hoechst 32558) and dried for microscopic analysis.

Western blotting. Western blotting was performed with the indicated amount of protein as previously described^{7,44,48,49}. Proteins were electrophoresed in an 8% sodium dodecyl sulfate mini gel and then electroblotted onto a nitrocellulose membrane in transfer buffer. Primary antibody at a specific dilution was used at 4°C overnight or at room temperature for 1 h. After washing with TBST (10 mM Tris-HCl, pH 7.8, 150 mM NaCl and 0.1% Tween 20), a horseradish peroxidase-conjugated secondary antibody at a dilution of 1:5000 dilution was applied to the membrane at room temperature for 1 h. After washing with TBS (10 mM Tris-HCl, pH 7.8, and 150 mM NaCl), a horseradish peroxidase-conjugated secondary antibody at a dilution of 1:5000 was applied to the membrane for 1 h at room temperature. Enhanced chemiluminescence detection of the target protein was performed using Western blotting detection reagents and X-ray film.

Immunoprecipitation (IP) and Western blotting. IP was performed using the Protein A beads method (DynaL Inc, Lake Success, NY) as exactly described by the manufacturer⁴⁸. Briefly, 200 µg of total protein was incubated for 2 h at 4°C with an antibody to target protein followed by incubation with protein A beads. After washing away unbound proteins, the immunoprecipitated protein complex was subjected to Western blotting for the proteins of interests. The procedures for Western blotting were exactly as described previously⁴⁴. Glyceraldehyde-3-phosphate dehydrogenase (GAPDH) was used as a protein loading control. The intensities of the bands were quantified using NIH Image J software.

Mass spectrometry analysis of pull down proteins. IP pull-down proteins were subjected to nanoHPLC-MS/MS as we previously described³⁹. The protein elutes were digested with 50 mM ammonium bicarbonate containing 200 ng of modified trypsin (Promega, Madison WI). Digestion was carried out overnight at 37°C after which the supernatant was collected, concentrated to approximately 10 µl and analyzed by nanoHPLC-MS/MS using a Q-TOF Ultima (Waters, Milford, MA). The entire samples were injected onto a 0.3 × 5 mm C18 micro pre-column cartridge (Dionex/LC-Packings) which was then brought online with a 75 µm × 50 mm Picofrit nanocolumn (New Objective, Woburn, MA) packed with BioBasic® C18 reversed phase media. The peptides were separated using a gradient supplied by a Waters CapLC pump (5–40% acetonitrile, 0.2% formic acid in 25 min, ~300 nL/min flow rate). The mass spectrometer was set to automatically acquire MS/MS spectra on doubly, triply and quadruply charged ions. Database searching was carried out in batch mode using Mascot Daemon™ (Matrix Science, London, U.K.) against the NCBI protein sequence database. All search returns were confirmed manually.

siRNA design and transfection. Two siRNAs targeting to Mical1, Mical2, respectively, were designed, tested and commercially synthesized by Santa Cruz Biotechnology (USA). Mical1 (sc-95537; Lot No: K0408), Mical2 (sc-96854; Lot No: L3108) and control siRNA (sc-36869; Lot No J2412) were the most effective in down-regulating Mical proteins through empirical selection after transfection into RBECs. The annealed double-stranded siRNAs at 0.3 to 1 µg/well (Falcon 24-well plate) were transfected into RBECs using a Lipofectamine 2000 (Invitrogen) transfection reagent kit, following the manufacturer's instructions. After 60 h or 72 h of transfection, cells were either fixed with 4% paraformaldehyde for morphological examination or collected for protein analysis using Western blotting.

Ratiometric calcium imaging. Intracellular calcium concentrations of Sema3A treated RBECs were measured using a technique exactly as we have previously described⁵⁰.

Mouse blood collection and Gr1 labelling. Mice (C57BL/6) were anesthetised and the chest was opened through the right ventricle and the blood was collected with a 3 ml 22 G3/4 syringe into EDTA tubes. Whole mouse blood at 0.5 ml was incubated with anti-Mouse Gr1 antibody for 1 h at room temperature. Following incubation, the blood sample was washed once in RPMI media supplemented with 0.5% BSA and re-suspended gently in 1 ml of RPMI supplemented with 0.5% BSA.

In vitro transwell assay. For the transwell migration assay: Each cell culture insert (12 mm, polycarbonate 3.0 µm, Millipore) was coated with 10 µg/ml bovine plasma fibronectin (ScienCell Research Laboratories, Carlsbad, CA) in Hank's balanced salt solution for 2 h at room temperature. RBECs at 1×10^5 were seeded on each cell culture insert in 0.25 ml F-12K media and the inserts were placed in a 24 well plate. After 48 h, RBECs were incubated with Sema3A at 5 µg/ml and 10 µg/ml concentrations for 1 h. Following incubation with Sema3A, the cell culture inserts were transferred to new wells and Gr1 labelled mouse blood sample (40 µl) in 210 µl of culture media was added to the upper well of the inserts. Following 2.5 h incubation, 100 µl of medium from the bottom well, containing the Gr1 transmigrated PMNs, was taken and quantified using a fluorescence microplate reader (FLx800, Bio-Tek) with Ex₆₅₀/Em₇₁₀ filter set. Fresh media (100 µl) was added to the bottom well. After additional 2 h, the fluorescence of Gr1 labelled transmigrated polymorphonuclear neutrophils (PMNs) from the bottom well was assessed again.

Permeability was also measured using [¹⁴C]sucrose serving as an additional control of barrier tightness besides the measurement of PMN transmigration. Radiolabeled [¹⁴C]sucrose (342 MW, 2.5 µCi, Amersham Biosciences, Piscataway, NJ) was applied to the RBEC monolayer after exposure to various concentrations of Sema3A. [¹⁴C]sucrose was applied to the apical compartment of the transwell and radiolabelled [¹⁴C]sucrose was collected from the bottom well after 2.5 and 4.5 h. Radioactivity was counted on a Beckman Model LS 5000 TD counter (Beckman Instruments, Fullerton, CA). Permeability was calculated as a percentage ratio (R) of the amount of radioactivity loaded to the apical chamber (C_{Top}) to the bottom chamber (C_{bottom}) and expressed as $R = (C_{\text{bottom}}/C_{\text{Top}}) \times 100$.

MMP2/9 gelatin Zymography. Brain tissue was freshly collected, homogenized in a buffer solution containing 50 mM Tris-HCl, 150 mM NaCl, 1% Nonidet P-40, 0.1% SDS, 0.1% deoxycholic acid (pH 7.4), and protease inhibitors. Protein concentrations were analyzed with a Bio-Rad system (Hercules, CA). Equal amounts of protein (20 µg/lane) for each sample were mixed with 2 X sample buffer and loaded on a 10% polyacrylamide gel incorporated with 0.1% gelatin for electrophoresis. MMP2 and MMP9 zymographic standards were used as positive controls (Chemicon). After electrophoresis, gels were washed in 2.5% Triton X-100 for 1 h, incubated for 18 h at 37°C in collagenase buffer, and stained for 1 h with 0.1% Coomassie brilliant blue dye. Gelatinolytic activity was visualized as a transparent band against a blue background and the band intensity was measured using Image J to quantify MMP2 and MMP9 activities.

Data analysis. Statistical analysis was performed using an unpaired Student's *t*-test with a 2-tailed *p* value, or using an ANOVA with Tukey's *post hoc* test for multiple comparisons using GraphPad Prism 5 from the GraphPad Software, Inc. (La Jolla, CA). In cases as specified, a non-parametric Mann-Whitney U test was performed. Differences were considered significant when the *p* value was less than 0.05, with * indicating *p* < 0.05 and ** indicating *p* < 0.01. All experiments were independently repeated at least three times. All values were expressed as mean ± S.E.M.

Results

Sema3A induces peripheral vasculature permeability. To determine if Sema3A increases blood vessel permeability, a Miles's assay was performed on the skin of anesthetized rats. Sema3A was injected intradermally into the shaved rat abdominal skin, or the rat ear skin which is semi-translucent and excellent for visualization of micro-circulation. PBS or VEGF were used as controls. As shown in Fig. 1(A, B, C), both VEGF and Sema3A caused increased extravasation of the Evans blue dye into the tissue compared to PBS-injected tissue, indicating an increased vascular permeability. Importantly, Sema3A induced vascular permeability were dose- and time-dependent (Fig. 1D–G). Quantitative analysis of Evans blue dye retained in the bleeding area demonstrated significantly increased vascular leakage of the dye after injection with Sema3A (Fig. 1C, E, G; ***p* < 0.01 compared to the PBS-treated group). Together, these data showed that Sema3A elevated permeability of peripheral vasculature.

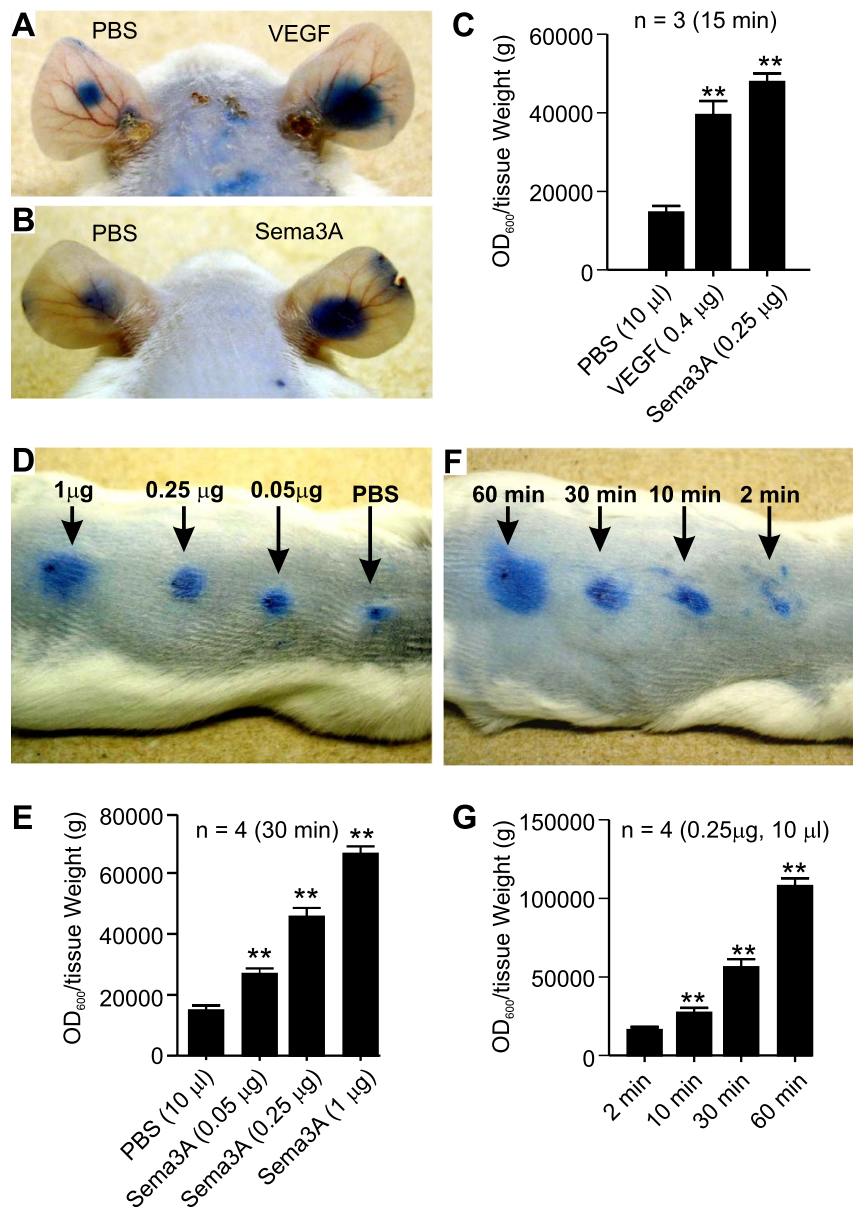


Figure 1 | Sema3A elevates peripheral vasculature permeability. The Mile's assay was performed on rat ears (A, B) and shaved abdominal skin (D, F). Rats were first injected with Evans blue dye through the lateral tail vein followed by an injection of 10 μ l of PBS, VEGF or Sema3A on the skin with the concentration and time as indicated. After thorough transcardial perfusion with saline to remove the Evans blue dye, the tissue containing residual Evans blue dye was removed surgically. Evans blue was extracted as described in the Methods section. The OD reading against tissue weight was calculated and shown in graphs C, E and G. At least three independent repeats were performed and ** indicates statistical significant with $p < 0.01$ by one-way ANOVA followed by Tukey's *post hoc* analysis to identify significant groups.

Sema3A elevates cerebrovascular permeability. We examined whether Sema3A plays a role in affecting the permeability of the cerebrovasculature, as its anatomical structure is more complex than that of the peripheral vasculature system. To this end, Sema3A was stereotactically injected into mouse cerebral cortex with a Bregma coordination of 0.9 mm lateral, 0.1 mm posterior, and -2.0 mm ventral using a Hamilton microsyringe at 1 μ l/min at a dosage of 200 ng/2 μ l. After thorough perfusion with saline, the residual Evans blue dye left in the brain tissue was quantified. Injection of PBS produced a small bleeding area over 60 min, serving as a baseline control for needle injury-induced blood vessel leakiness (Fig. 2A top panel, B). In contrast, injecting VEGF or Sema3A caused a much higher degree of bleeding in the cerebral cortex after 30 min and 60 min (Fig. 2A, B, $p < 0.01$ compared to PBS treatment). Most importantly, injecting Sema3A into mouse

brain lacking the expression of endogenous Sema3A (Sema3A^{-/-} mouse) also produced elevated vascular permeability. The increased level of permeability occurred in Sema3A^{-/-} mouse brain was similar to that of the Sema3A^{+/+} mice over the same time course (Fig. 2A bottom panel and B, $p > 0.05$, not significant). This experiment indicates that exogenous Sema3A was capable of inducing vascular permeability in the absence of endogenous Sema3A.

To further demonstrate that Sema3A elevates vascular permeability, Sema3A was over-expressed in Sema3A^{+/+} and Sema3A^{-/-} littermate mice brain using replication defective adenovirus expressing an eGFP-tagged Sema3A (Ad-Sema3A-eGFP). Ad-Sema3A-eGFP was injected into the lateral tail vein. After 3 d of infection, mouse brain was subjected to Western blot. As shown in Fig. 2(C and D), significant increase in Sema3A protein level occurred in Ad-Sema3A-eGFP infected Sema3A^{+/+} and Sema3A^{-/-} mice brain

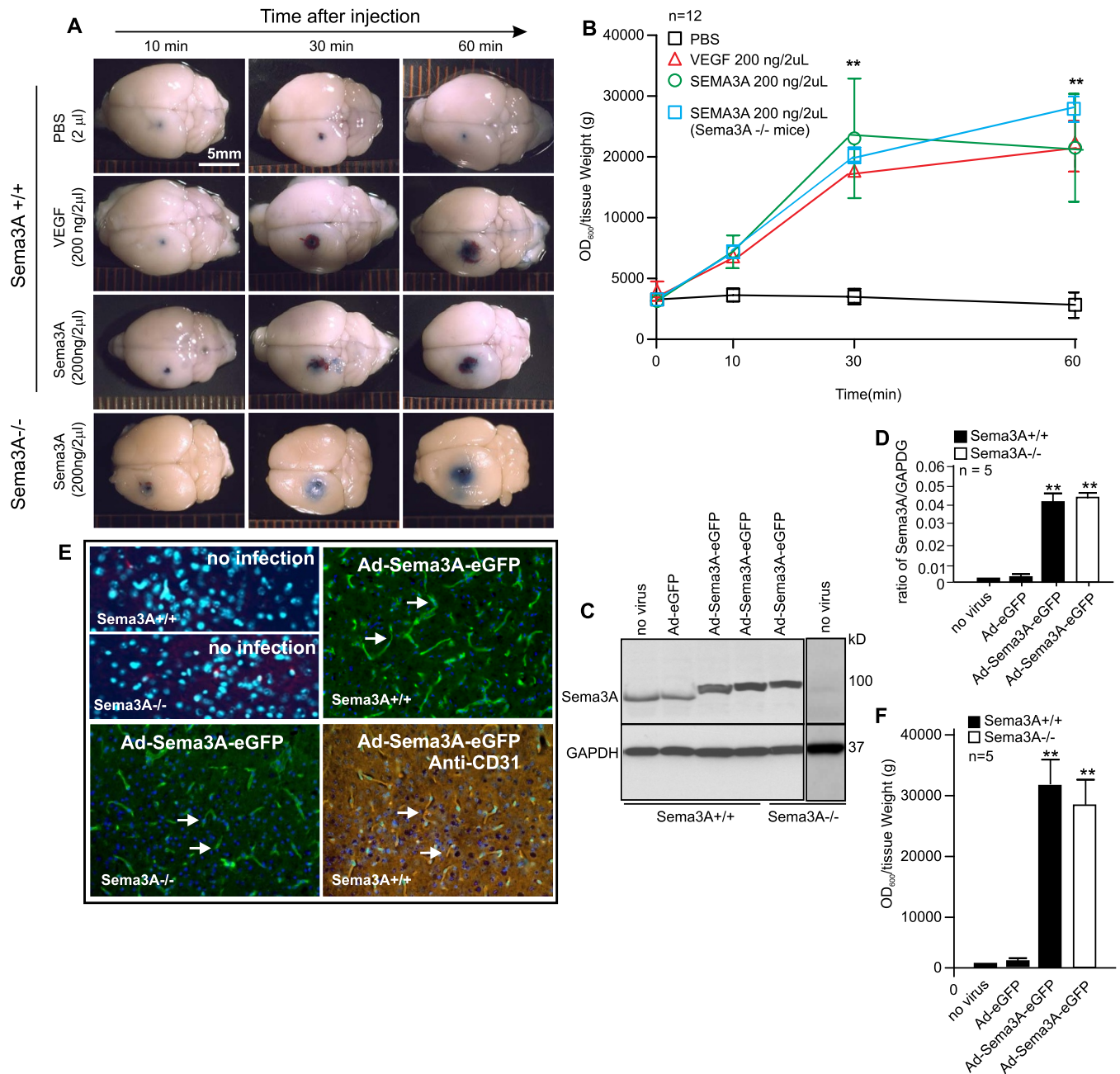


Figure 2 | Sema3A elevates cerebrovascular permeability. Sema3A^{+/+} mice were injected with Evans blue through the lateral tail vein, followed by a stereotactical injection with PBS, VEGF, or Sema3A with the amount and time as indicated in panel A. Sema3A^{-/-} mice were also treated similarly to show increased vascular permeability when endogenous Sema3A was absent. After thorough transcardial perfusion with saline to remove Evans blue dye, the tissue containing residual Evans blue dye in the brain was surgically cut out and extracted as described in the Methods section. Quantification of permeability (OD of Evans blue/tissue weight) was shown in panel B. Statistics were performed as indicated in the Methods section with ** indicating $p < 0.01$ against the PBS-injected brains. Panels C–E: Replication defective adenovirus expressing Sema3A (Ad-Sema3A-eGFP) was injected into the brain through the lateral tail vein. After 3 d of infection, mice were injected with Evans blue and the brain residual Evans blue was quantified after a thorough transcardial perfusion with saline. Ad-eGFP-injected brain and no virus injected mouse brain were used as controls. Western blotting was performed to show increased Sema3A expression in the brain (C). The cropped blots are shown in the figure and the full-length blots are presented in supplementary figure S1. Quantification of Sema3A expression was performed using Image J (D). Brain section was stained with DAPI to visualize brain cells (blue color in E) and EGFP positive blood vessels (green color in E). Anti-CD31 staining (Rhodamine, red color) was performed on Ad-Sema3A-eGFP injected brain to indicate endothelial expression of Sema3A (yellow color in E lower right hand panel). Cerebrovascular permeability was determined by injecting Evans blue through the lateral tail vein. After transcardial perfusion with saline, brain residual Evans blue was quantified as shown in F. ** indicates $p < 0.01$ compared to the no virus treatment group. Scale bars = 80 μ m.

($p < 0.01$, compared with Ad-eGFP infected group). Sema3A expression increased mostly on the endothelial cells of cerebrovasculature, as confirmed by the presence of eGFP green color (Fig. 2E) and by double labeling of blood vessels with an anti-CD31 antibody

(Fig. 2E lower right hand panel, yellow color indicates vessels expressing eGFP and CD31). Importantly, the vascular permeability increased in both Sema3A^{+/+} and Sema3A^{-/-} mice brains in comparison with Ad-eGFP infected mice (Fig. 2F; $p < 0.01$). Collectively,

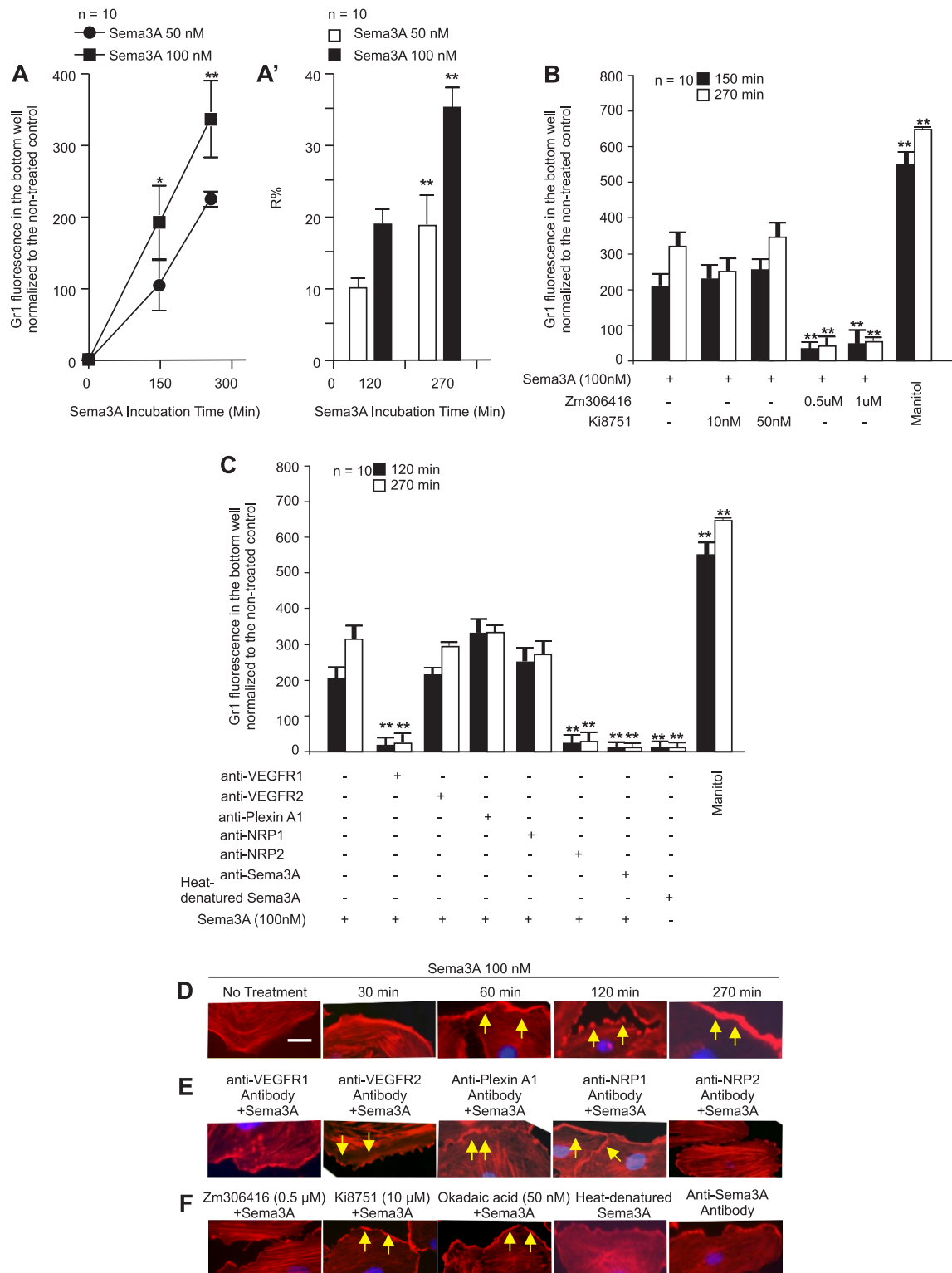


Figure 3 | Sema3A induces permeability of endothelial cells *in vitro*. Cultured RBECs were grown on a transwell to a confluent monolayer. After treating the transwell with Sema3A (as indicated in A), or pre-treating cells with antibodies or inhibitors against known Sema3A receptors as indicated in B and C, freshly prepared mouse blood labeled with fluorescent Gr1 antibody (to label PMNs) was applied onto the transwell to perform permeability assay. [14 C]sucrose was also used for transwell assay to detect paracellular permeability in response to Sema3A (A'; $p < 0.01$ compared with the 120 min treatment group). The effect of a battery of inhibitors and antibodies against Sema3A receptors was also tested using the PMN permeability assay. ** indicating $p < 0.01$ by one-way ANOVA with Tukey's *post hoc* analysis compared with Sema3A treatment group. Panels D – F show morphological changes of RBEC cells due to Sema3A treatment. RBECs were fixed after the indicated treatment and stained with phalloidin conjugated with rhodamine (red color) and counter stained with DAPI (blue color). F-actin stress fibres are very clear in untreated cells (D). Sema3A treatment caused disruption of F-actin inside the cells. Densely packed bundles of cortical actin filaments started to appear along cell membranes (arrows) over the course of treatment with Sema3A. Antibodies and inhibitors against receptors of Sema3A were pre-incubated with the cells for 15 min before the addition of Sema3A. Antibodies to VEGFR1 and NRP2 (panel E) and the inhibitor Zm 306416 (selective to VEGFR1, panel F) were effective in ameliorating the effect of Sema3A. Scale bar = 20 μ m.

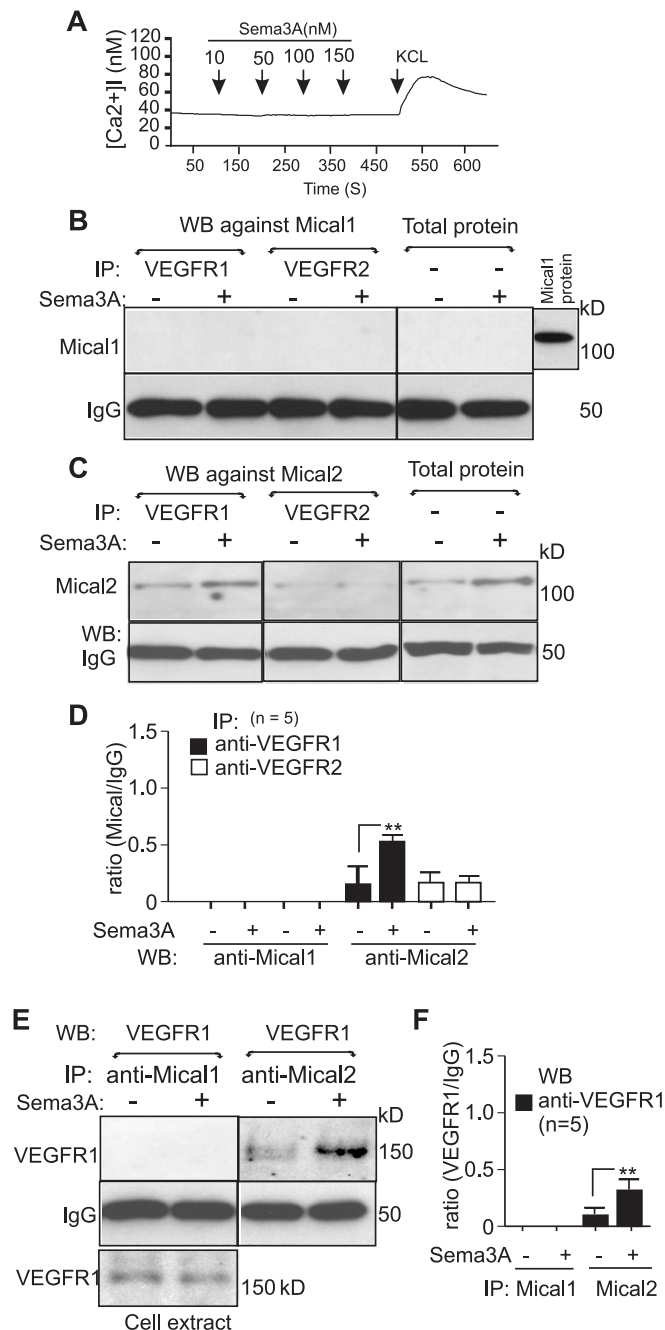


Figure 4 | VEGFR1 directly interacts with Mical2 in response to Semaphorin 3A. (A) Cultured RBEC cells were grown on glass cover slips and treated with Sema3A at 10, 50, 100 and 150 nM and the intracellular calcium concentrations were measured. KCl was added to cells which caused a drastic increase in intracellular calcium due to depolarization of cellular membrane. (B) Cultured RBECs were treated with Sema3A and followed by protein extraction as described in the Methods section. Protein isolations were immunoprecipitated with antibodies to VEGFR1 or VEGFR2 (B, C) and followed by Western blotting against Mical1 (B; the right side lane is recombinant Mical1 protein from Abnova, serving as a positive control) or Mical2 (C). Total Mical2 proteins were probed as loading controls. Western blot against IgG of the same gel was also performed to show equal protein loading as an internal control. The cropped blots are shown in the figure and the full-length blots are presented in supplementary figure S2 and S3. (D) Western blot images were measured using Image J and the band intensity was normalized against the respective IgG band of the same sample. The result of three repeats was averaged and plotted in D. (E) A reverse immunoprecipitation-Western

blot was performed, in that Sema3A treated RBEC cell protein lysates were immunoprecipitated with antibodies against Mical1 or Mical2 and blotted with an antibody against VEGFR1. IgG was detected as an internal control. Cell total lysate was probed with an antibody to VEGFR1 (bottom blot of E). The cropped blots are shown in the figure and the full-length blots are presented in supplementary figure S4. Quantification of the VEGFR1 band against IgG is shown in F. Increased VEGFR1, but not VEGFR2, associated with Mical2 occurred in response to Sema3A treatment (average of three experiments as shown in F). ** indicates statistical significant with $p < 0.01$ by Student's t -test.

these experiments demonstrated that Sema3A indeed plays a role in elevating the permeability of cerebrovasculature.

Sema3A elevates permeability in an in vitro model of blood brain barrier (BBB). To determine the mechanisms underlying Sema3A-induced vascular permeability, we used RBEC cultured on transwell to determine the permeability of fluorescent-labeled Gr1 positive polymorphonuclear neutrophils (PMNs). This assay is a powerful tool to investigate mechanisms of BBB permeability⁵¹. Indeed, as shown in Fig. 3A, Sema3A caused a dose- and time-dependent increase in transmigration of the PMNs across the RBEC monolayer of cells, demonstrating elevated permeability.

Radiolabeled [¹⁴C]sucrose was also performed on RBEC serving as an additional control of barrier tightness besides the measurement of PMN transmigration. Since [¹⁴C]sucrose is not subjected to transporters or taken up by endothelial cells, it can only permeate to the corresponding chamber in the transwell system via the paracellular pathway. Indeed, as shown in Fig. 3A', exposing RBEC cells to various concentrations of Sema3A increased the permeability of radiolabeled [¹⁴C]sucrose in a similar pattern and to a similar degree compared to those of PMN transmigration assay (Fig. 3A). This experiment thereby confirmed the validity of PMN transmigration assay to monitor RBEC permeability, at least in the current experimental condition. Subsequently, all permeability experiments were performed using the PMN assay.

Sema3A interacts with VEGFRs to mediate vasculogenesis and vascular patterning. To understand whether Sema3A-evoked permeability also involves in its cognate receptors, several VEGFR specific inhibitors were used before Sema3A treatment in the PMN paracellular transmigration assay. Sema3A-induced paracellular permeability of RBEC was blocked by ZM 306416, an inhibitor for VEGFR1 with a known IC_{50} of 0.33 μ M (Fig. 3B; $p < 0.01$ compared to Sema3A treatment group). In contrast, Ki8751, a potent and selective inhibitor of VEGFR2 with a known IC_{50} of 0.9 nM, was not effective at 10 nM and 50 nM; suggesting that Sema3A elevates paracellular permeability through VEGFR1. In addition, cantharidin, a potent and selective PP2A inhibitor known to affect Sema3A-mediated vasculogenesis, and other known Sema3A intracellular downstream kinase inhibitors such as okadaic acid, LY294002 and Y-27632, were also not effective (not shown), serving as negative controls to demonstrate that Sema3A selectively interacts with VEGFR1 to mediate RBEC paracellular permeability. Mannitol caused shrinkage of the RBEC and maximum paracellular permeability serving as a positive control for maximum barrier leakiness.

To further confirm the involvement of specific receptors for Sema3A-induced permeability, a battery of receptor specific antibodies were used. Preliminary experiments were performed using Western blot to demonstrate the specificities of these antibodies recognizing their respective receptors (not shown). Moreover, these antibodies alone neither altered the cellular morphology seen under phalloidin staining, nor changed RBEC permeability to PMNs (not shown). As shown in Fig. 3C, antibodies blocking VEGFR1 and NRP2 were effective in ameliorating Sema3A-induced permeability to PMNs; while Sema3A pre-mixed with the antibody against Sema3A or heat-denatured Sema3A did not cause increased per-

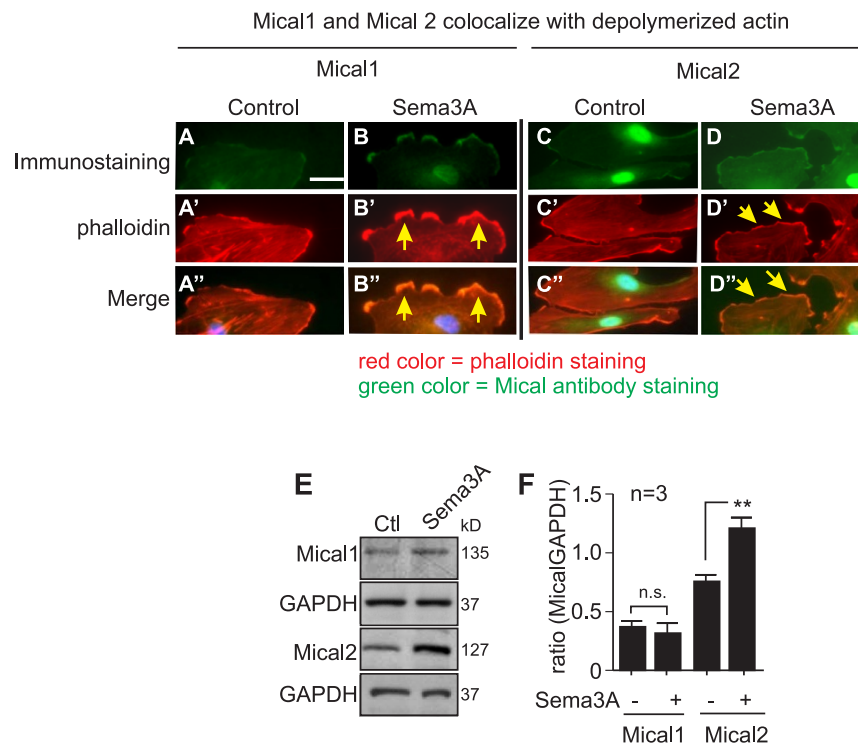


Figure 5 | Co-localization of Mical proteins with cortical actin filaments in the membrane ruffles. Immunostaining for Mical1 (green color in A, B) and Mical 2 (green color in C, D) was performed on cultured RBEC cells treated with Sema3A. Phalloidin staining (A' - D'; red color) was also performed to indicate the location of actin. Merged images of Mical protein immunostaining with phalloidin are shown in A'' - D''. Arrows indicate co-localized Mical proteins with cortical actin filaments (yellow color in A'' - D''). Scale bar = 50 μ m. Expression of Mical1 and Mical2 was also determined using Western blot (E) and quantified using Image J (F). ** indicates statistical significant with $p < 0.01$ by Student's *t*-test. The cropped blots are shown in the figure and the full-length blots are presented in supplementary figure S5.

meability to PMNs, serving as negative controls (Fig. 3C; $p < 0.01$ compared to Sema3A treatment group). Together, these data confirmed VEGFR1/NRP2 as receptors for Sema3A during Sema3A-induced permeability.

We then examined morphological changes of RBEC in response to Sema3A treatment using phalloidin staining of F-actin. Sema3A treated cells exhibited a marked alteration in cell shape, an apparent loss of polarity and a distorted actin cytoskeleton over the course of treatment (30–270 min at 100 nM of Sema3A) (Fig. 3D). Intracellular cytoplasmic actin stress fibers (F-actin) began to form densely packed bundles of cortical actin filaments in the membrane ruffles, first in the shape of sawtooth-like bodies along the cell membrane (arrows in Fig. 3D), then as a thick layer of densely packed bundles of cortical actin filaments in the membrane ruffles (Fig. 3D). This change in actin cytoskeleton and cellular morphology could lead to the disruption of intracellular junctions and increased paracellular permeability as reported by others⁵².

To determine the specificity of Sema3A-induced actin changes, RBECs were treated either with heat-denatured Sema3A, or a Sema3A pre-mixed with antibody to Sema3A. Both failed to produce a dramatic actin response to Sema3A (Fig. 3F), confirming the specificity of cellular response to Sema3A. RBECs were also pre-treated with specific antibodies to VEGFR1, VEGFR2, Plexin A1, NRP1, NRP2, or VEGFR inhibitors including Zm306416, Ki8751 and okadaic acid to further delineate receptors responsible for Sema3A-induced actin filament changes (Fig. 3E and F). As shown in Fig. 3E and F, blocking RBEC with antibodies to VEGFR1, NRP2 and Ki8751 ameliorated the appearance of Sema3A-induced densely packed bundles of cortical actin filaments close to the membrane. While antibodies to VEGFR2, Plexin A1, NRP1, Ki8751 and okadaic acid did not prevent the appearance of Sema3A-induced actin changes.

Together, these studies showed that Sema3A induces disruption of intracellular actin filaments and causes shrinkage of endothelial cells, through VEGFR1/NRP2 receptors.

VEGFR1 directly interacts with Mical2 to mediate Sema3A response. To further explore how Sema3A induces F-actin distortion, we designed and performed the following two experiments. First, ratiometric calcium concentration was measured to determine whether Sema3A directly increases intracellular calcium, which is known to modulate actin filament changes^{53,54}. As shown in Fig. 4A, Sema3A at 10, 50, 100, and 150 nM concentrations failed to elicit any measurable changes in intracellular calcium concentration of RBEC. KCl was used as a positive control, which depolarized the cellular membrane and produced a non-specific influx of intracellular calcium (Fig. 4A). This experiment excluded the possibility that Sema3A causes F-actin disorganization through modulating intracellular calcium levels.

Secondly, experiments were performed to determine what intracellular proteins that VEGFR1 directly interacts with to mediate Sema3A response. Immunoprecipitation with an antibody to VEGFR1 was performed on Sema3A-treated RBECs followed by mass spectrometry analysis. We identified Mical2 protein as a potential intracellular target of VEGFR1 (Mascot Score = 120; peptide count = 17; cover percentage = 30.86%). Indeed, immunoprecipitation-Western blotting was performed on VEGFR1 pull-down product, which confirmed the presence of Mical2 (Fig. 4C). To validate the finding that VEGFR1 directly interacts with Mical2 in response to Sema3A treatment, Sema3A-treated RBECs were immunoprecipitated with an antibody to VEGFR1 or VEGFR2, followed by Western blotting against Mical1 (Fig. 4B) or Mical 2 (Fig. 4C). After quantification of the relative intensities of the Western blot

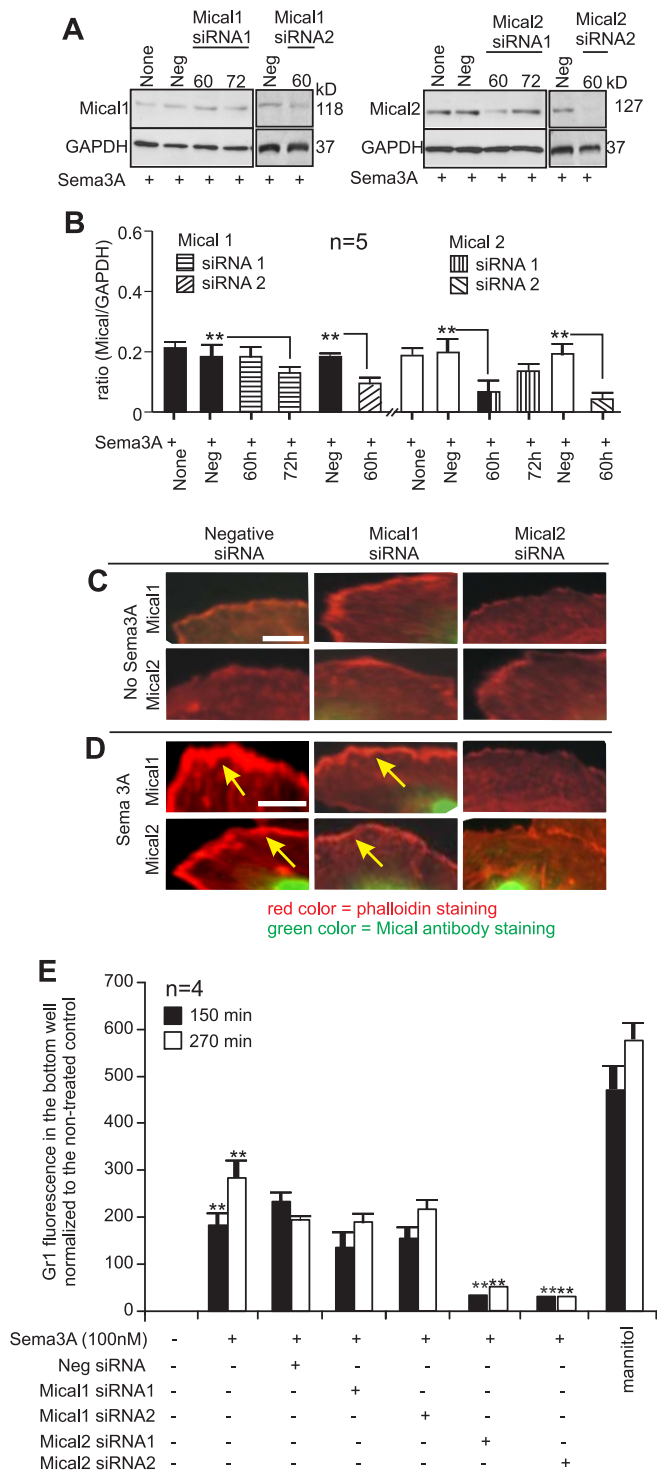


Figure 6 | Mical2 is required for Sema3A-induced actin disorganization and permeability. siRNAs to Mical1 and Mical2 were transfected into RBECs (A). Western blot was performed to determine the reduction of Mical protein over the course of transfection (A and B). Immunostaining was performed to detect the presence of Mical proteins (C and D, green color). After 60 h or 72 h of transfection with siRNA, cells were treated with or without Sema3A for determination of formation of cortical actin filaments (arrows in D). siRNA to Mical2 inhibited Sema3A-induced Mical2 expression and prevented the accumulation of densely packed bundles of cortical actin filaments close to the membrane (arrows indicate cortical actin filaments). (E) RBECs placed on transwells were transfected with siRNAs against Mical1 or Mical2. After 60 h of transfection, permeability to Gr1-labelled PMNs from fresh mouse blood was

determined for 150 min and 270 min treatment with Sema3A. Mannitol was used as a positive control to indicate maximum permeability to PMNs. siRNA to Mical2 effectively reduced Sema3A induced permeability to PMNs.

** indicates statistical significant with $p < 0.01$ by one-way ANOVA with *post hoc* Tukey's test compared with Sema3A-treated, negative siRNA transfected group.

bands as shown in Fig. 4D, it was clear that VEGFR1 increased binding with intracellular Mical2 in response to Sema3A treatment ($p < 0.01$).

To confirm that VEGFR1 binds to Mical2, RBECs treated with or without Sema3A were immunoprecipitated with antibodies to Mical1 or Mical2 and followed by Western blotting with the antibody to VEGFR1 (Fig. 4E and F). Indeed, Mical2, but not Mical1, showed a strong interaction with VEGFR1 in response to Sema3A treatment (Fig. 4E and F; $p < 0.01$). These studies demonstrated unequivocally that VEGFR1 interacts with Mical2 in signaling the endothelial cells' response to Sema3A.

Mical2 is required for Sema3A-induced disorganization of F-actin and permeability. To demonstrate whether Mical2 is required for Sema3A-induced F-actin changes and permeability, three experiments were designed and performed (Fig. 5). First, co-immunostaining of Mical1 and Mical2 with actin filaments was performed. As shown in Fig. 5A, C and E, untreated RBECs have low level of expression of Mical1 and Mical2. After treatment with Sema3A, Mical2 expression level increased (Fig. 5D, E and F; $p < 0.01$), while Mical1 levels remained almost unchanged (Fig. 5B, E, and F; $p = 0.14$, n.s.). Increased Mical2 co-localized with densely packed bundles of cortical actin filaments close to the membrane in Sema3A-treated cells (Fig. 5C', C'', D' and D''). Mical1 did not appear to increase in cortical actin filaments (Fig. 5A', A'', B' and B'').

Secondly, down-regulation of Mical2 prevents F-actin disorganization in response to Sema3A treatment. Specific siRNAs to Mical1 and Mical2 (two each) were transfected into RBECs. A non-specific siRNA was also used as a negative control. The siRNA1 and siRNA2 to Mical2 selectively knocked down Mical2 protein expression after 60 h of transfection in response to Sema3A treatment (Fig. 6A and B; $p < 0.01$). Double immunostaining of Mical1, or Mical2 with phalloidin (F-actin) showed that the appearance of cortical actin filaments occurred in the negative siRNA and Mical1 siRNA transfected cells in response to Sema3A, but not in cells transfected with Mical2 siRNA (Fig. 6C and D), which strongly supports the hypothesis that Mical2 mediates actin filament disorganization in response to Sema3A.

Thirdly, transwell assay was performed to determine if knock-down of Mical2 expression was indeed able to reduce Sema3A-induced endothelial permeability to Gr1-labelled PMNs. As shown in Fig. 6E, both siRNAs knocking down Mical2, but not Mical1, were effective in preventing Sema3A-induced permeability, presumably by reducing changes in cellular morphology due to the inhibition of actin filament disorganization. Together, these three experiments demonstrated that Mical2 is responsible for Sema3A-induced F-actin disorganization and permeability.

Knockout Sema3A protects the brain from ischemia-induced damage. We previously showed that Sema3A expression was elevated 6 h after transient occlusion of the middle cerebral artery (tMCAO). The high level of Sema3A expression persisted during long term reperfusion^{6,8,9}. If Sema3A plays a role in augmenting vascular permeability during tMCAO, knockout Sema3A expression could reduce vascular permeability and provide brain protection. To test these hypotheses, two types of cerebral ischemia, i.e. tMCAO and photothrombotic occlusion/hemorrhagic transformation, were induced on Sema3A +/+ and Sema3A -/- littermate mice.

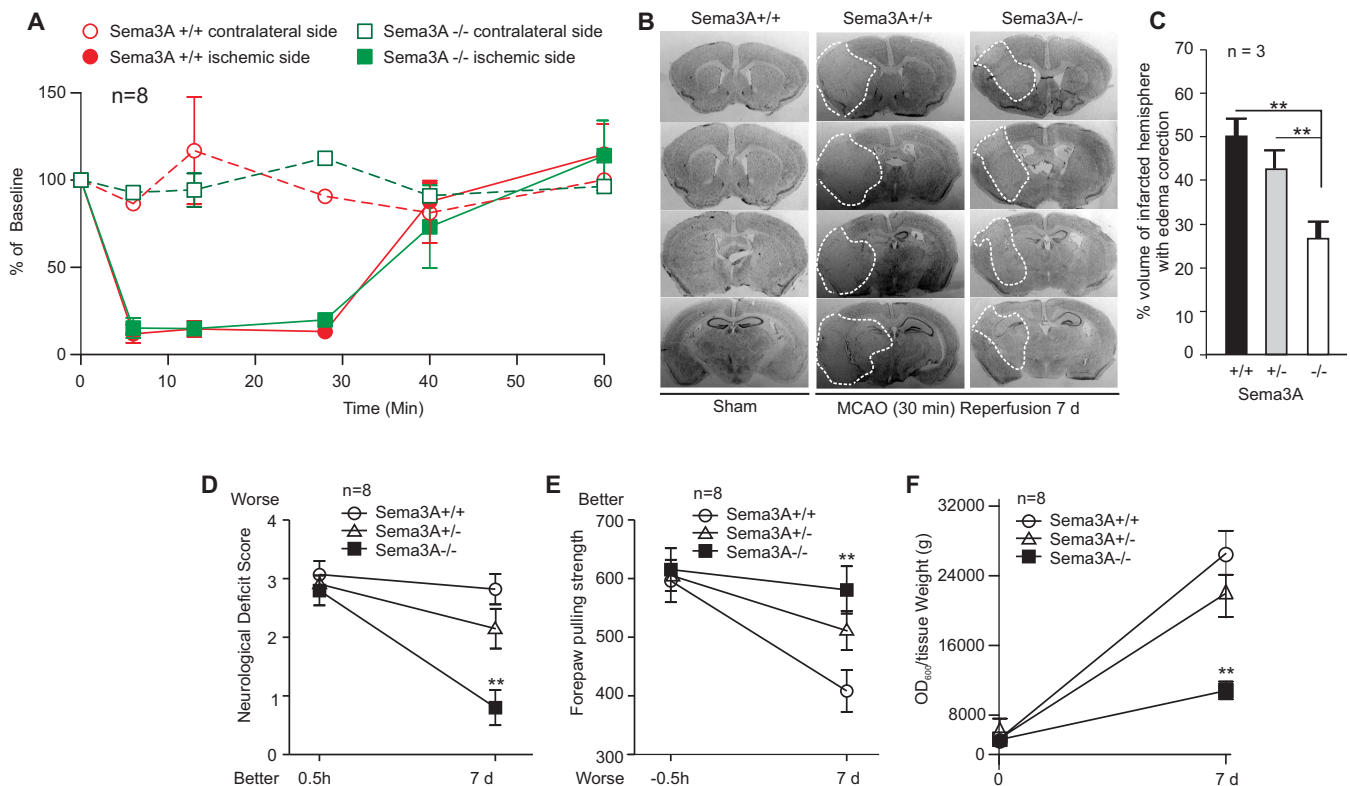


Figure 7 | Sema3A $^{-/-}$ mice have reduced brain infarction following tMCAO. (A) Middle cerebral artery blood flow was monitored using laser Doppler flowmetry. Transient occlusion of the middle cerebral artery reduced blood flow by 90% in Sema3A $+/+$ and Sema3A $-/-$ mice. Removal of the occluding thread resorted blood flow to near normal level in both types of mice. (B) After 7 d of tMCAO-reperfusion, mice were killed and the brains were freshly frozen. Brain sections were cut and stained using crystal violet. Circled areas on the coronal sections indicate ischemic infarction. (C) The infarct volume was quantified using Image J by measuring serial sections. ** indicates statistical significance with $p < 0.01$ by one-way ANOVA with Tukey's *post hoc* analysis against Sema3A $+/+$ mouse brains. (D) The neurological deficit scores were recorded 0.5 h after tMCAO and 7 d post tMCAO. (E) The pulling strength of the forepaws was also measured 0.5 h before tMCAO and 7 d post tMCAO. ** indicates $p < 0.01$ compared with Sema3A $+/+$ mice. (F) To determine vascular permeability in Sema3A $-/-$ mice following tMCAO, Evans blue dye was injected through the tail vein 15 min before sacrificing tMCAO mice. After a thorough transcardial perfusion with saline, brain tissue was extracted to determine the level of residual amount of Evans blue. Sema3A $-/-$ mice showed significantly lower vascular permeability caused by tMCAO at 7 d post stroke. ** indicates $p < 0.01$ compared with Sema3A $+/+$ mice.

As Sema3A is a known inhibitor of angiogenesis and vascular patterning during development, we first compared the density of cortical cerebral microvessels of adult Sema3A $+/+$ and $-/-$ littermate mice (19–21 g body weight and at least 2 weeks after weaning). Lectin staining was performed on brain sections (not shown). Although Sema3A $-/-$ mice appeared to have a slightly higher density of cerebral microvessels, the vascular density was not significantly different from that seen in Sema3A $+/+$ mice brain (not shown). Indeed, a measurement of the basal level of the middle cerebral artery blood flow for both Sema3A $+/+$ and $-/-$ mice showed no significant difference (Fig. 7A, $p = 0.23$). Occlusion of the middle cerebral artery of both Sema3A $+/+$ and $-/-$ mice produced a similar level reduction in blood flow (90%) (Fig. 7A). The blood flow was restored to almost 100% after withdrawal of the occluding thread in both Sema3A $+/+$ and $-/-$ littermate mice. Interestingly, Sema3A $-/-$ mice produced a statistically significant smaller infarct after tMCAO (Fig. 7B and C; $p < 0.01$), and a better neurological deficit score (Fig. 7D; $p < 0.05$), and forepaw pulling strength test (Fig. 7E; $p < 0.05$) compared with Sema3A $+/+$ littermate mice, suggesting that Sema3A plays a detrimental role during cerebral ischemia. To determine if Sema3A $-/-$ mice had reduced vascular permeability, Evans blue was injected through the tail vein after tMCAO. After a thorough transcardial perfusion with saline, Sema3A $-/-$ ischemic mouse brain had a significantly reduced level of the Evans blue compared with the Sema3A $+/+$ littermate mice (Fig. 7F; $p < 0.01$), confirming reduced vascular permeability.

To further demonstrate the role of Sema3A *in vivo*, another mouse stroke model, i.e. photothrombotic occlusion/hemorrhagic transformation, was used to show reduced brain injury due to the lack of Sema3A expression. As shown in Fig. 8A, this model produces vascular occlusions mostly in the cortical layer. With experimentally pre-determined illuminating light strength and duration, a well-defined and quantifiable damage volume was achieved as determined by TTC staining (Fig. 8B). On brain sections subjected to hematoxylin and eosin (H&E) staining, ischemic occlusion was followed by hemorrhagic transformation (Fig. 8C, arrowheads indicating occluded vessels, arrows indicating spilled blood cells in the brain due to hemorrhage). Sema3A $-/-$ mice showed a significantly smaller infarct volume compared with the Sema3A $+/+$ mice (Fig. 8A and B; $p < 0.01$). Importantly, Sema3A $-/-$ mouse brain had a significantly reduced level of hemorrhagic transformation (Fig. 8C and D; $p < 0.01$).

In order to confirm that Sema3A $-/-$ mouse brain has reduced brain damage and vascular permeability during photothrombotic occlusion/hemorrhagic transformation injury, the following three experiments were performed; (1) We have previously showed that the level of CRMP3 proteolytic cleaved product p54 is associated with the degree of brain damage^{39,40,44}. Therefore, the level of p54 was determined using Western blot. The level of p54 was higher in Sema3A $+/+$ + ischemic side of the brain compared with the Sema3A $-/-$ brain (Fig. 8E and F), suggesting stronger brain damage in Sema3A $+/+$ brain. The level of residual hemoglobin (after thorough brain per-

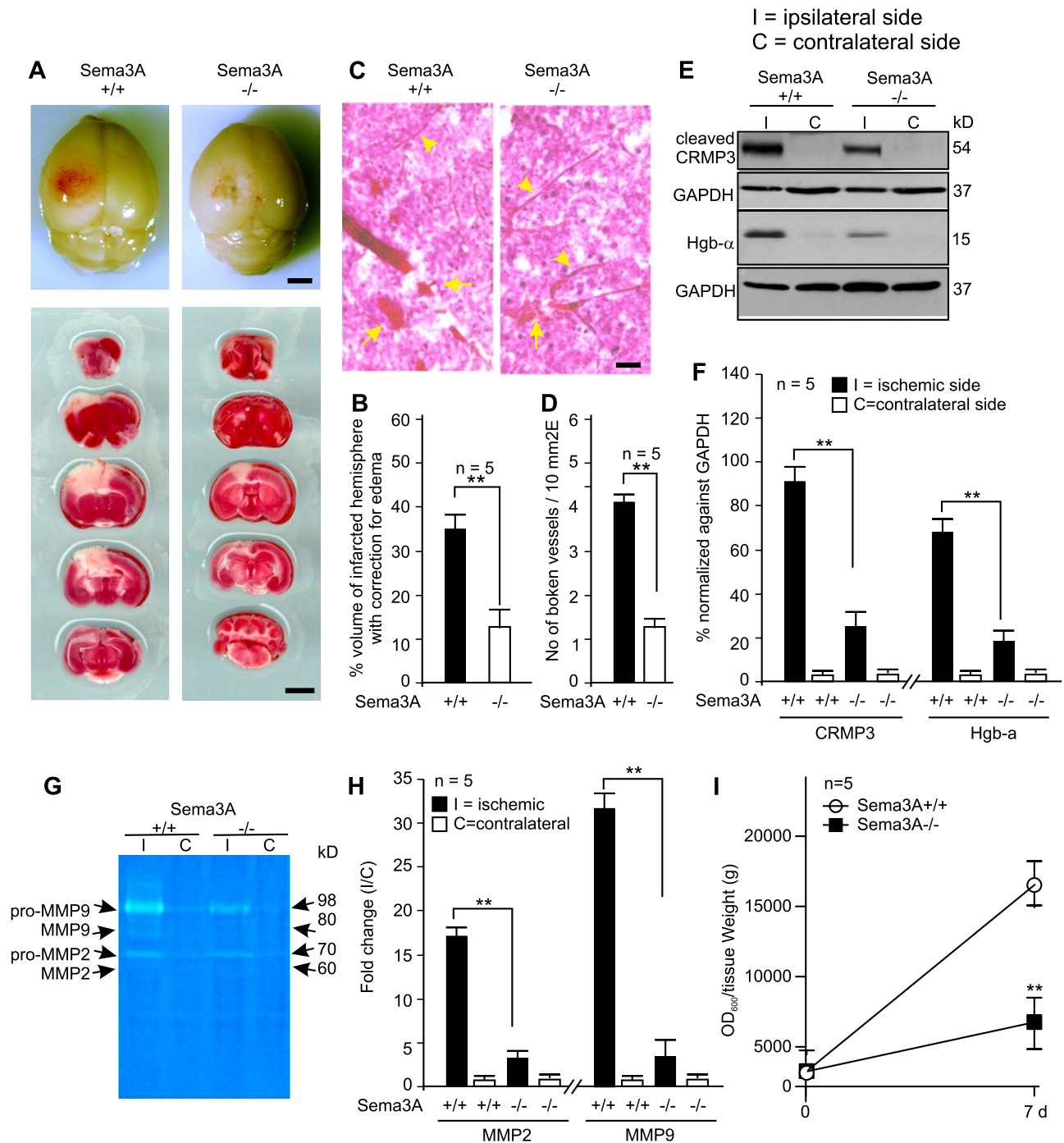


Figure 8 | Sema3A $^{-/-}$ mice have reduced vascular permeability and brain damage in photothrombotic occlusion/hemorrhagic transformation model. Sema3A $+/+$, $-/-$ littermate mice were subjected to the same surgical procedure to produce ischemic occlusion/hemorrhagic transformation in the brain as described in the Methods section. As shown in A (top panels), blood left in the brain (red color) was visible even after perfusion (scale bar = 10 mm). Thick coronal sections (2 mm) were stained with TTC to show brain infarction (white area in the lower panels of A, scale bar = 15 mm). This infarction in Sema3A $+/+$ mice were significantly larger than that of Sema3A $-/-$ mice (B, ** indicates $p < 0.01$). Brain sections were stained with H&E to show elevated presence of blood cells in the brain parenchyma (arrows in C) indicating increased hemorrhagic transformation in this model. Arrowheads in C show occluded, but non-hemorrhagic vessels. The number of broken blood vessels were counted and plotted in D to indicate significantly reduced vascular damage in Sema3A $-/-$ mouse brain. (E) Brain tissue was subjected to protein isolation and Western blot to detect proteolytic cleaved CRMP3 (54 kD band, p54), and the residual hemoglobin (Hgb- α) in the brain. GAPDH was used as an internal control. I = ipsilateral side of the brain, while C = contralateral side of the brain. The cropped blots are shown in the figure and the full-length blots are presented in supplementary figure S6. (F) Image J was used to quantify Western blot band intensities from panel E. ** indicates $p < 0.01$. (G) Gelatin zymography was performed on brain protein samples to detect pro-MMP2/9 (98 and 70 kD, respectively) and activated MMP2/9 (80 and 60 kD, respectively). (H) The band intensity was measured using Image J. ** indicates $p < 0.01$. (I) Evans blue was injected into mouse brain 15 min before sacrifice. After thorough transcardial perfusion with saline, mouse brain was taken out and residual Evans blue was quantified using methods described in the Methods section. Sema3A $-/-$ mice showed significantly reduced level of Evans blue in the ischemic brain (** indicates $p < 0.01$; $n = 3$).



fusion with saline), indicating hemorrhagic transformation, were also measured using Western blotting (Fig. 8E and F). *Sema3A*^{-/-} mouse brain showed reduced presence of residual hemoglobin compared with a *Sema3A*^{+/+} brain (Fig. 8E and F; $p < 0.01$), demonstrating reduced brain damage in the *Sema3A*^{-/-} mouse. (2) Gelatin zymography was performed to show reduced activation of MMP2 and MMP9, both are important markers for vascular damage and permeability. As shown in Fig. 8G and H, the levels of activated MMP2 and 9 increased significantly in the ischemic side of the brain of *Sema3A*^{+/+} mouse ($p < 0.05$), but not in the *Sema3A*^{-/-} mouse brain, lending further support to the notion that *Sema3A* modulates vascular permeability. (3) Ischemic mice were injected with Evans blue after 7 d of ischemic surgery. After a thorough transcardial perfusion, residual Evans blue in the brain was quantified as shown in Fig. 8I. *Sema3A*^{-/-} mice had a significantly lower level of residual Evans blue in the brain ($p < 0.01$), which again demonstrated that *Sema3A* plays a role in augmenting vascular permeability in the ischemic brain.

Collectively, these studies provided *in vitro* and *in vivo* evidence to show that *Sema3A* indeed modulates vascular permeability to affect brain damage after cerebral ischemia. Ischemic brain tissue secretes *Sema3A* which binds to the VEGFR1/NRP2 complex to trigger the activation of Mical2. Mical2 co-localizes with actin filaments and disorganize F-actin bundles into densely packed bundles of cortical actin filaments close to the membrane leading to the alteration of endothelial cell morphology. The cellular integrity of endothelial cells is critical in guarding the vascular permeability.

Discussion

In the present study, we provided evidence to demonstrate that *Sema3A* is a vascular permeability factor and contributes to ischemic brain damage. By interacting with the VEGFR1/NRP2 receptor complex, *Sema3A* triggers the activation of Mical2 to cause disorganization of F-actin, alteration of cellular morphology, and elevation of the endothelial permeability. It is especially important that the *Sema3A*^{-/-} mouse has reduced vascular permeability in response to two types of stroke *in vivo*, all resulting in a better protection of the brain tissue and function in comparison with the *Sema3A*^{+/+} littermate mouse. Collectively, these data strongly supports the notion that *Sema3A* induces stroke brain damage through elevation of vascular permeability.

We employed Mile's assay⁵⁵ to show that exogenous *Sema3A* elevated the permeability of both peripheral and cerebral vasculatures. Importantly, exogenous *Sema3A* injected into mice lacking of endogenous *Sema3A* (*Sema3A*^{-/-}) also evoked elevated permeability of cerebrovasculature (Fig. 2A), confirming the specificity of *Sema3A*'s action. Comparing *Sema3A*'s effect in vascular permeability with that caused by VEGF₁₋₁₆₅ using the Mile's assay, it became apparent that *Sema3A* is as potent as VEGF in the degree of inducing vascular permeability. This is perhaps not surprising in light of the fact that *Sema3A* triggers vascular permeability through VEGFR1 (with NRP2 as a partner). It may be highly possible that VEGF and *Sema3A* share the same receptor complex and compete with each other in mediating vascular permeability. Indeed, it is known that during development, *Sema3A* competes with VEGF in receptor binding to mediate vascular patterning^{56,57}. Alternatively, expressions of *Sema3A* and VEGF are discretely regulated spatiotemporally during the progression of brain ischemic injury to exert the same effect on elevating vascular permeability through shared VEGFR/NRP receptor complexes. Future studies are warranted. Nevertheless, this is the first study to establish a role for *Sema3A* in vascular permeability in the adult ischemic brain.

The molecular mechanism for *Sema3A*-mediated vascular permeability is through activation of Mical2 protein, which in turn causes F-actin disorganization. This process appears to be selective, since Mical1 expression did not become elevated in response to

Sema3A treatment. Down-regulation of Mical1 using siRNA also did not show any effect on endothelial cell F-actin disorganization and permeability. Mical2 protein, on the other hand, is required in shaping endothelial cell F-actin organization, confirming a previous study in fruit fly, in that Mical2 links Semaphorin to F-actin disassembly^{34,35}. However, our finding that Mical2 protein-mediated actin changes affect human endothelial permeability is novel. F-actin plays such an important role in maintaining tight and adherence junction proteins in place. Ample studies have clearly shown that the disruption of cytoskeleton, including actin filaments, will increase BBB permeability^{52,58–60}. Therefore, it is reasonable to conclude that *Sema3A* enhances endothelial permeability as a result of Mical2-mediated disorganization of F-actin and the loss of endothelial cell shape and polarity.

Our *in vitro* data predicts that *Sema3A* secreted in the ischemic brain exacerbates vascular permeability. Indeed, mice lacking the expression of functional *Sema3A* (*Sema3A*^{-/-}) showed a significant reduction in vascular permeability and brain damage in two models of cerebral ischemia. *Sema3A* is the only member of the semaphorin family as a secreted polypeptide. Based on our previous published studies, *Sema3A* expression in ischemic brain during reperfusion is relatively evenly diffused in the ischemic core and its adjacent area^{6,7,61}, which may account for the striking reduction in vascular permeability of the ischemic hemisphere shown in Fig. 7 and 8. It is especially interesting to see *Sema3A*^{-/-} mice also having reduced hemorrhagic transformation in the brain, which further supports an important role of *Sema3A* as a vascular permeability factor. Future studies are required to determine how exactly *Sema3A* causes hemorrhagic transformation.

Nevertheless, brain protection seen in *Sema3A*^{-/-} mice can also be attributed to direct neuroprotection. Our previous studies showed that *Sema3A* can directly interact with NRP1 receptors, but not NRP2 receptors, expressed on neurons to cause neuronal death both *in vitro* and *in vivo* in ischemic brain^{5,7,8,62}. Perhaps, *Sema3A* interacts with different receptor complexes to discretely impact neurons and the vasculature. Indeed, studies showed that the cellular target of *Sema3A* is very selective, as it only inhibits the outgrowth of a specific set of neurons such as spinal motor neurons and neurons in the embryonic dorsal root ganglion and sympathetic ganglion^{63–65}, lending further support to the notion that *Sema3A*'s effect on vascular permeability is separate from its effect on neuronal death possibly through interacting with different receptor complexes. In fact, *Sema3A* released from ischemic neuron has been reported to inhibit vascular regeneration¹⁹. Moreover, *Sema3A* inhibition alleviates ischemia-reperfusion-induced acute kidney injury⁶⁶. Therefore, *Sema3A* plays a very important role in a diverse disease conditions through affecting vascular homeostasis.

Collectively, these studies revealed a previously unknown function of *Sema3A* in mediating vascular permeability in ischemic brain. The possible mechanism is through its selective interaction with VEGFR1/NRP2 receptor complex to cause F-actin disorganization and alteration of endothelial cell shape, polarity and permeability.

1. Siegenthaler, J. A., Sohet, F. & Daneman, R. 'Sealing off the CNS': cellular and molecular regulation of blood-brain barrier genesis. *Curr. Opin. Neurobiol.* **23**, 1057–1064 (2013).
2. Gursoy-Ozdemir, Y., Yemisci, M. & Dalkara, T. Microvascular protection is essential for successful neuroprotection in stroke. *J. Neurochem.* **123** Suppl 2, 2–11 (2012).
3. Maki, T. *et al.* Biphasic mechanisms of neurovascular unit injury and protection in CNS diseases. *CNS. Neurol. Disord. Drug Targets.* **12**, 302–315 (2013).
4. Rhim, T., Lee, D. Y. & Lee, M. Drug Delivery Systems for the Treatment of Ischemic Stroke. *Pharm. Res.* **30**, 2429–2444 (2013).
5. Hou, S. T., Jiang, S. X. & Smith, R. A. Permissive and repulsive cues and signalling pathways of axonal outgrowth and regeneration. *Int. Rev. Cell Mol. Biol.* **267**, 125–181 (2008).
6. Hou, S. T. *et al.* Sustained up-regulation of semaphorin 3A, Neuropilin1, and doublecortin expression in ischemic mouse brain during long-term recovery. *Biochem. Biophys. Res. Commun.* **367**, 109–115 (2008).



7. Jiang, S. X., Sheldrick, M., Desbois, A., Slinn, J. & Hou, S. T. Neuropilin-1 is a direct target of the transcription factor E2F1 during cerebral ischemia-induced neuronal death in vivo. *Mol. Cell Biol.* **27**, 1696–1705 (2007).
8. Jiang, S. X. *et al.* Neuropilin 1 directly interacts with Fer kinase to mediate semaphorin 3A-induced death of cortical neurons. *J. Biol. Chem.* **285**, 9908–9918 (2010).
9. Whitehead, S. N., Gangaraju, S., Slinn, J. & Hou, S. T. Transient and bilateral increase in Neuropilin-1, Fer kinase and collapsin response mediator proteins within membrane rafts following unilateral occlusion of the middle cerebral artery in mouse. *Brain Res.* **1344**, 209–216 (2010).
10. Beck, H. *et al.* Cell type-specific expression of neuropilins in an MCA-occlusion model in mice suggests a potential role in post-ischemic brain remodeling. *J. Neuropathol. Exp. Neurol.* **61**, 339–350 (2002).
11. Carmichael, S. T. Cellular and molecular mechanisms of neural repair after stroke: making waves. *Ann. Neurol.* **59**, 735–742 (2006).
12. Fujita, H., Zhang, B., Sato, K., Tanaka, J. & Sakanaka, M. Expressions of neuropilin-1, neuropilin-2 and semaphorin 3A mRNA in the rat brain after middle cerebral artery occlusion. *Brain Res.* **914**, 1–14 (2001).
13. Zhang, Z. G., Tsang, W., Zhang, L., Powers, C. & Chopp, M. Up-regulation of neuropilin-1 in neovasculature after focal cerebral ischemia in the adult rat. *J. Cereb. Blood Flow Metab.* **21**, 541–549 (2001).
14. Pekcec, A. *et al.* Following experimental stroke, the recovering brain is vulnerable to lipoxigenase-dependent semaphorin signaling. *FASEB J.* **27**, 437–445 (2013).
15. Le, G. A. *et al.* Semaphorin 3A elevates endothelial cell permeability through PP2A inactivation. *J. Cell Sci.* **125**, 4137–4146 (2012).
16. De Winter, F., Holtmaat, A. J. & Verhaagen, J. Neuropilin and class 3 semaphorins in nervous system regeneration. *Adv. Exp. Med. Biol.* **515**, 115–139 (2002).
17. Pasterkamp, R. J. & Giger, R. J. Semaphorin function in neural plasticity and disease. *Curr. Opin. Neurobiol.* **19**, 263–274 (2009).
18. Duh, E. J. Sema 3A resists retinal revascularization. *Blood* **117**, 5785–5786 (2011).
19. Joyal, J. S. *et al.* Ischemic neurons prevent vascular regeneration of neural tissue by secreting semaphorin 3A. *Blood* **117**, 6024–6035 (2011).
20. Luo, Y., Raible, D. & Raper, J. A. Collapsin: a protein in brain that induces the collapse and paralysis of neuronal growth cones. *Cell* **75**, 217–227 (1993).
21. Luo, Y. *et al.* A family of molecules related to collapsin in the embryonic chick nervous system. *Neuron* **14**, 1131–1140 (1995).
22. Steup, A. *et al.* Semaphorin D acts as a repulsive factor for entorhinal and hippocampal neurons. *Eur. J. Neurosci.* **11**, 729–734 (1999).
23. Serini, G. *et al.* Class 3 semaphorins control vascular morphogenesis by inhibiting integrin function. *Nature* **424**, 391–397 (2003).
24. Carmeliet, P. & Tessier-Lavigne, M. Common mechanisms of nerve and blood vessel wiring. *Nature* **436**, 193–200 (2005).
25. Acevedo, L. M., Barillas, S., Weis, S. M., Gothert, J. R. & Cheresh, D. A. Semaphorin 3A suppresses VEGF-mediated angiogenesis yet acts as a vascular permeability factor. *Blood* **111**, 2674–2680 (2008).
26. Maione, F. *et al.* Semaphorin 3A is an endogenous angiogenesis inhibitor that blocks tumor growth and normalizes tumor vasculature in transgenic mouse models. *J. Clin. Invest.* **119**, 3356–3372 (2009).
27. Guttman-Raviv, N. *et al.* Semaphorin-3A and semaphorin-3F work together to repel endothelial cells and to inhibit their survival by induction of apoptosis. *J. Biol. Chem.* **282**, 26294–26305 (2007).
28. He, Z. & Tessier-Lavigne, M. Neuropilin is a receptor for the axonal chemorepellent Semaphorin III. *Cell* **90**, 739–751 (1997).
29. Kolodkin, A. L. *et al.* Neuropilin is a semaphorin III receptor. *Cell* **90**, 753–762 (1997).
30. Gu, C. *et al.* Neuropilin-1 conveys semaphorin and VEGF signaling during neural and cardiovascular development. *Dev. Cell* **5**, 45–57 (2003).
31. Hota, P. K. & Buck, M. Plexin structures are coming: opportunities for multilevel investigations of semaphorin guidance receptors, their cell signaling mechanisms, and functions. *Cell Mol. Life Sci.* **69**, 3765–3805 (2012).
32. Soker, S., Takashima, S., Miao, H. Q., Neufeld, G. & Klagsbrun, M. Neuropilin-1 is expressed by endothelial and tumor cells as an isoform-specific receptor for vascular endothelial growth factor. *Cell* **92**, 735–745 (1998).
33. Eliceiri, B. P. *et al.* Selective requirement for Src kinases during VEGF-induced angiogenesis and vascular permeability. *Mol. Cell* **4**, 915–924 (1999).
34. Hung, R. J. *et al.* Mical links semaphorins to F-actin disassembly. *Nature* **463**, 823–827 (2010).
35. Hung, R. J., Pak, C. W. & Terman, J. R. Direct redox regulation of F-actin assembly and disassembly by Mical. *Science* **334**, 1710–1713 (2011).
36. Giridharan, S. S., Rohn, J. L., Naslavsky, N. & Caplan, S. Differential regulation of actin microfilaments by human MICAL proteins. *J. Cell Sci.* **125**, 614–624 (2012).
37. Zhou, Y., Gunput, R. A., Adolfs, Y. & Pasterkamp, R. J. MICALs in control of the cytoskeleton, exocytosis, and cell death. *Cell Mol. Life Sci.* **68**, 4033–4044 (2011).
38. Taniguchi, M. *et al.* Disruption of semaphorin III/D gene causes severe abnormality in peripheral nerve projection. *Neuron* **19**, 519–530 (1997).
39. Hou, S. T. *et al.* Calpain-cleaved collapsin response mediator protein-3 induces neuronal death after glutamate toxicity and cerebral ischemia. *J. Neurosci.* **26**, 2241–2249 (2006).
40. Jiang, S. X. *et al.* Calpain cleavage of collapsin response mediator proteins in ischemic mouse brain. *Eur. J. Neurosci.* **26**, 801–809 (2007).
41. Watson, B. D., Dietrich, W. D., Busto, R., Wachtel, M. S. & Ginsberg, M. D. Induction of reproducible brain infarction by photochemically initiated thrombosis. *Ann. Neurol.* **17**, 497–504 (1985).
42. Zhao, B. Q. *et al.* Essential role of endogenous tissue plasminogen activator through matrix metalloproteinase 9 induction and expression on heparin-produced cerebral hemorrhage after cerebral ischemia in mice. *Blood* **103**, 2610–2616 (2004).
43. Whitehead, S. N. *et al.* Imaging mass spectrometry detection of gangliosides species in the mouse brain following transient focal cerebral ischemia and long-term recovery. *PLoS. One.* **6**, e20808 (2011).
44. Hou, S. T., Jiang, S. X., Aylsworth, A., Cooke, M. & Zhou, L. Collapsin response mediator protein 3 deacetylates histone H4 to mediate nuclear condensation and neuronal death. *Sci. Rep.* **3**, 1350 (2013).
45. Hou, S. T., Jiang, S. X., Huang, D. & Desbois, A. A novel adenoviral vector-mediated neuronal selective gene expression in neonatal mouse brain in response to hypoxia. *Neurosci. Lett.* **419**, 23–27 (2007).
46. Huang, D., Desbois, A. & Hou, S. T. A novel adenoviral vector which mediates hypoxia-inducible gene expression selectively in neurons. *Gene Ther.* **12**, 1369–1376 (2005).
47. Nakagawa, S. *et al.* A new blood-brain barrier model using primary rat brain endothelial cells, pericytes and astrocytes. *Neurochem. Int.* **54**, 253–263 (2009).
48. Hou, S. T. *et al.* CaMKII phosphorylates collapsin response mediator protein 2 and modulates axonal damage during glutamate excitotoxicity. *J. Neurochem.* **111**, 870–881 (2009).
49. Jiang, S. X., Slinn, J., Aylsworth, A. & Hou, S. T. Vimentin participates in microglia activation and neurotoxicity in cerebral ischemia. *J. Neurochem.* **122**, 764–774 (2012).
50. Jiang, S. X. *et al.* Chlortetracycline and demeclocycline inhibit calpains and protect mouse neurons against glutamate toxicity and cerebral ischemia. *J. Biol. Chem.* **280**, 33811–33818 (2005).
51. Gangaraju, S. *et al.* Cerebral endothelial expression of Robo1 affects brain infiltration of polymorphonuclear neutrophils during mouse stroke recovery. *Neurobiol. Dis.* **54**, 24–31 (2013).
52. Cristante, E. *et al.* Identification of an essential endogenous regulator of blood-brain barrier integrity, and its pathological and therapeutic implications. *Proc. Natl. Acad. Sci. U. S. A.* **110**, 832–841 (2013).
53. Dawson, J. F., Sablin, E. P., Spudich, J. A. & Fletterick, R. J. Structure of an F-actin trimer disrupted by gelsolin and implications for the mechanism of severing. *J. Biol. Chem.* **278**, 1229–1238 (2003).
54. Saneyoshi, T. & Hayashi, Y. The Ca²⁺ and Rho GTPase signaling pathways underlying activity-dependent actin remodeling at dendritic spines. *Cytoskeleton (Hoboken.)* **69**, 545–554 (2012).
55. Senger, D. R. Tumor cells secrete a vascular permeability factor that promotes accumulation of ascites fluid. *Science* **219**, 983–985 (1983).
56. Miao, H. Q. *et al.* Neuropilin-1 mediates collapsin-1/semaphorin III inhibition of endothelial cell motility: functional competition of collapsin-1 and vascular endothelial growth factor-165. *J. Cell Biol.* **146**, 233–242 (1999).
57. Soker, S., Miao, H. Q., Nomi, M., Takashima, S. & Klagsbrun, M. VEGF165 mediates formation of complexes containing VEGFR-2 and neuropilin-1 that enhance VEGF165-receptor binding. *J. Cell Biochem.* **85**, 357–368 (2002).
58. Ivanov, A. I. Actin motors that drive formation and disassembly of epithelial apical junctions. *Front. Biosci.* **13**, 6662–6681 (2008).
59. Vandenbroucke, E., Mehta, D., Minshall, R. & Malik, A. B. Regulation of endothelial junctional permeability. *Ann. N. Y. Acad. Sci.* **1123**, 134–145 (2008).
60. Anderson, J. M. & Van Itallie, C. M. Physiology and function of the tight junction. *Cold Spring Harb. Perspect. Biol.* **1**, a002584 (2009).
61. Hou, S. T., Jiang, S. X. & Smith, R. A. Permissive and repulsive cues and signalling pathways of axonal outgrowth and regeneration. *Int. Rev. Cell Mol. Biol.* **267**, 125–181 (2008).
62. Hou, S. T., Jiang, S. X., Slinn, J., O'Hare, M. & Karchewski, L. Neuropilin 2 deficiency does not affect cortical neuronal viability in response to oxygen-glucose-deprivation and transient middle cerebral artery occlusion. *Neurosci. Res.* **66**, 396–401 (2010).
63. Nakamura, F., Kalb, R. G. & Strittmatter, S. M. Molecular basis of semaphorin-mediated axon guidance. *J. Neurobiol.* **44**, 219–229 (2000).
64. Nakamura, F., Tanaka, M., Takahashi, T., Kalb, R. G. & Strittmatter, S. M. Neuropilin-1 extracellular domains mediate semaphorin D/III-induced growth cone collapse. *Neuron* **21**, 1093–1100 (1998).
65. Sandvig, A., Berry, M., Barrett, L. B., Butt, A. & Logan, A. Myelin-, reactive glia-, and scar-derived CNS axon growth inhibitors: expression, receptor signaling, and correlation with axon regeneration. *Glia* **46**, 225–251 (2004).
66. Ranganathan, P., Jayakumar, C., Mohamed, R., Weintraub, N. L. & Ramesh, G. Semaphorin 3A inactivation suppresses ischemia-reperfusion-induced inflammation and acute kidney injury. *Am. J. Physiol. Renal Physiol.* **307**, F183–F194 (2014).

Acknowledgments

We thank Dr Masahiko Taniguchi (Sapporo Medical University, Japan) for the kind gift of the Sema3A knockout mouse, IBS Animal Facility for the timely supply of experimental animals. This work was supported by grant-in-aid from the Heart and Stroke Foundation of



Ontario (NA5393, T5760, and T6706), Canadian Institutes of Health Research (CCI-85680), a SUSTC startup fund, a grant from the Science and Technology Innovation Commission of Shenzhen Municipality (JCYJ20140417105742709), and a State Key Laboratory of Neuroscience Open Compete Project (SKLN-201403) to S.T.H.

Author contributions

S.T.H. conceived and designed the experiments, analyzed the data and wrote the manuscript. L.N. performed Evans blue dye brain injection and assay, L.N. performed brain tissue sectioning and immunostaining; X.S.L. performed the Mile's assay and quantification; brain surgery, RBEC treatment, acquired images and analyzed some of the data; J.S. performed tMCAO stroke surgery and S.X.J. performed neurological deficit analysis; A.A. performed IP and siRNA studies; S.G. performed PMN transmigration assay

using RBECs, S.X.J. and R.M. performed calcium imaging and photothrombotic model work.

Additional information

Supplementary information accompanies this paper at <http://www.nature.com/scientificreports>

Competing financial interests: The authors declare no competing financial interests.

How to cite this article: Hou, S.T. *et al.* Semaphorin3A elevates vascular permeability and contributes to cerebral ischemia-induced brain damage. *Sci. Rep.* 5, 7890; DOI:10.1038/srep07890 (2015).



This work is licensed under a Creative Commons Attribution-NonCommercial-NoDerivs 4.0 International License. The images or other third party material in this article are included in the article's Creative Commons license, unless indicated otherwise in the credit line; if the material is not included under the Creative Commons license, users will need to obtain permission from the license holder in order to reproduce the material. To view a copy of this license, visit <http://creativecommons.org/licenses/by-nc-nd/4.0/>